



Failure analysis of field-aged polymeric outdoor insulators and performance enhancement for electric stress using nonlinear field grading composites

M-Ramez Halloum¹ · B. Subba Reddy¹ · G. Nithin Reddy¹

Received: 3 October 2022 / Accepted: 14 June 2023 / Published online: 26 June 2023
© The Author(s), under exclusive licence to Springer-Verlag GmbH Germany, part of Springer Nature 2023

Abstract

Polymeric outdoor insulators are increasingly employed in transmission and distribution systems. The various electric and environmental stresses significantly affect their long-term performance due to their organic nature, leading to degradation and aging of the insulation materials. Experimental studies have been carried out on in-service polymeric outdoor insulators for more than 20 years (400 kV and 132 kV) to investigate the structural changes and the effects of these stresses on the degradation and aging of the housing material (silicone rubber). The silicone rubber was subjected to the following tests: Fourier transform infrared spectroscopy, scanning electron microscopy and energy-dispersive X-ray, and hydrophobicity measurements. In addition, the equivalent salt deposit density and non-soluble deposit density measurements and tensile strength measurements have been carried out. The results of the field-aged polymeric insulators are compared with fresh samples also. These investigations show some interesting results, which are presented and analyzed. Finally, a 2D axisymmetric model of the 132-kV insulator was developed using COMSOL Multiphysics and the finite element method. One mitigation technique for excessive electric stress was studied using field grading composite (FGM) based on zinc oxide microvaristors. Suitable electrical characteristics and an optimized design of field grading material have been proposed to effectively control the electric stress of the 132-kV polymeric outdoor insulators under various operating conditions. The results of the simulation demonstrate that using FGMs can significantly improve the performance of polymeric insulators in the field. Further development of FGM and experimental investigations are planned.

Keywords Polymeric outdoor insulator · SEM · EDAX · FTIR · Nonlinear resistive field grading material (FGM) · Finite element method (FEM) · Zinc oxide microvaristors

1 Introduction

Polymeric outdoor insulators are increasingly being used in power transmission and distribution systems, owing to their excellent features over traditional glass and ceramic insulators. One of the essential features is significant weight reduction, up to 90%. Moreover, excellent mechanical strength, little shattering, and less installation and maintenance costs while allowing for long service life. Furthermore, silicone rubber shows a superior hydrophobicity that inhibits the formation of a continuous conductive film along the surface of

the insulator under wet conditions and presents excellent performance under contamination/pollution. In comparison with traditional insulators (glass and ceramic), composite insulators are less susceptible to vandalism [1, 2].

Fiber-reinforced plastic (FRP) rods represent the primary component of polymeric outdoor insulators that provide internal insulation and bear mechanical loads. Silicone rubber (SiR) housing is used to protect the FRP rod against various environmental and electrical stresses. In addition, it gives the required creepage distance limiting the leakage current. SiR comprises polydimethylsiloxane (PDMS) with inorganic fillers such as aluminum trihydrate (ATH) to improve the tracking and erosion resistance [3]. In comparison with materials such as EVA, EPR, and EPDM with carbon backbones, silicone rubber with a siloxane (Si–O–Si) backbone offers better performance. Siloxanes

✉ M-Ramez Halloum
mramezh@iisc.ac.in

¹ High Voltage Laboratory, Department of Electrical Engineering, Indian Institute of Science, Bangalore, India

(silicon–oxygen–silicon) are more thermally stable than carbon–carbon chain polymers, which exhibit higher damage and degradation during tracking and arcing and release more carbonaceous compounds. Moreover, PDMS is hydrophobic due to the methyl group (CH₃) in the side chain providing better performance under wet conditions [4].

Polymeric outdoor insulators, on the other hand, have some drawbacks, because of their organic nature, they are more susceptible to degeneration and aging due to various environmental (dust, rain, light, and heat) and electrical stresses (E-field enhancements, leakage current, etc.) [5]. In [6, 7], the thermal degradation of polymeric insulators has been investigated by simultaneously applying thermal stress with UV radiation. Silicone rubber, however, is found to have good long-term UV-resistant behavior. The electric field profile along the insulator length is highly non-uniform due to its structure, where the electric field intensity is excessively high near both terminals. Localized field enhancements near the terminals of polymeric outdoor insulators result in premature degradation and aging of the insulation material due to dry and water-induced corona discharges [8]. Under wet-polluted environments, the performance of polymeric outdoor insulators is significantly reduced because of the formation of dry bands over the insulator surface. High current density and electric fields near both terminals lead to non-homogeneous drying of the insulator surface and thus forming dry bands. Therefore, strong electric field enhancements arise at the extremities of the dry bands due to the high dielectric constant of the wet pollution layer compared with insulation material and air. Dry bands' arcs lead to premature aging and erosion of insulation materials [9].

Field grading for polymeric insulators is highly desirable to avoid such unfavorable consequences and assure satisfactory performance in service. In general, there are two different types of field grading techniques, which are classified into either capacitive or resistive field grading depending on the nature of the dominant current (displacement or resistive current). Recently, new nonlinear resistive FGMs based on zinc oxide microvaristors have been demonstrated. These new composites have superior characteristics to the traditional FGMs based on carbon black or silicon carbide, allowing them to be used in high-voltage systems and providing more competitive products. Many investigations on various FGMs based on ZnO microvaristors have been recently published to alleviate electric field enhancements for a variety of HV applications, including power electronics modules [10], cable accessories (joints and terminations) [11], coils of HV generators and motors [12], and polymeric insulation systems [13–17]. Recent developments in compounding ZnO microvaristors with silicone rubber offer a promising approach for mitigating localized field enhancements in different HV applications [18–22]. These

new composites have high nonlinear field-dependent conductivity characteristics. Switching characteristics of FGMs, such as nonlinearity coefficient and field switching threshold, can be tailored specifically for a given application allowing for high flexibility for different HV applications. Since resistive field grading depends on the resistive current, care must be taken to avoid overheating and undesirable thermal consequences. The design and switching parameters of field grading materials have been proposed on a quantitative basis in the previous works [13–16]. Under normal operating conditions, however, if the active portions of FGMs are confined to a small region, local resistive field grading can be justified for a long time. With inappropriate switching characteristics, on the other hand, the heating consequences could result in detrimental thermal impacts. The FGMs design and switching characteristics must be precisely specified for a particular application to keep integral Joule heating to a minimum during continuous operation.

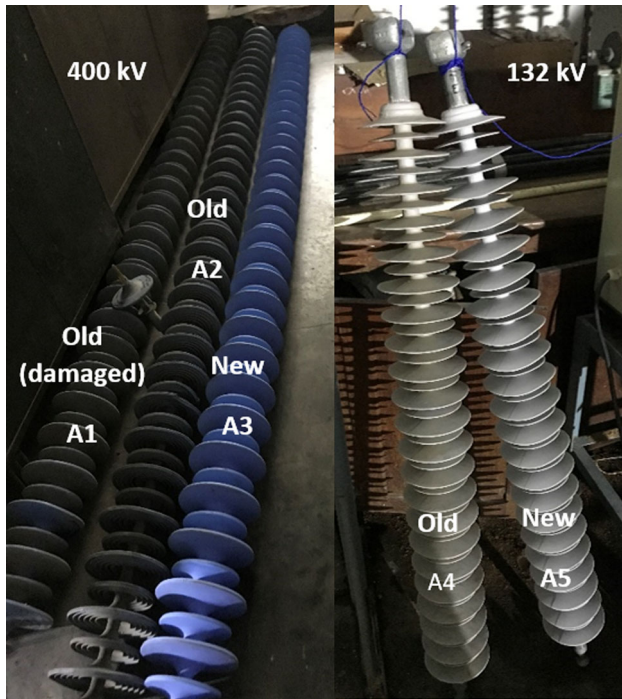
This paper aims to evaluate the microstructural changes of housing material of 132-kV and 400-kV field-aged polymer outdoor insulators and compare results with fresh samples. Investigations have been conducted on the housing material (silicone rubber) to present the effect of electrical stress (dry and water-induced corona discharges, dry band discharges, leakage current, etc.) and environmental stress (pollution, ultraviolet radiation, temperature, etc.) on the insulation material. The housing material was subjected to Fourier transform infrared spectroscopy (FTIR), scanning electron microscopy (SEM) and energy-dispersive X-ray (EDX), hydrophobicity measurements, equivalent salt deposit density (ESDD), non-soluble deposit density (NSDD), and tensile strength measurements. Finally, a 2D axisymmetric model of the 132-kV insulator was developed using COMSOL Multiphysics 5.5 and the finite element method (FEM). Suitable electrical characteristics and an optimized design of field grading material have been proposed to effectively control the electric stress of the 132-kV polymeric outdoor insulators under various operating conditions (dry and clean, wet and light pollution, wet and heavy pollution, with water droplets, and lightning impulse).

2 Experimentation details

Two different sets of field-aged polymeric insulators (400 kV and 132 kV) have been tested, which were in service for more than 20 years, as shown in Fig. 1. Table 1 shows the details of the tested insulators. This study has conducted different material tests on SiR housing materials to assess the SiR housing condition of field-aged polymeric outdoor insulators at the microscopic level. The details of the experimental tests and methods pertaining to the present investigation are illustrated below.

Table 1 The details of field-aged polymeric outdoor insulator samples

Sample no.	A1	A2	A3	A4	A5
Rating	400 kV			132 kV	
Condition	Old (damaged)	Old	New	Old	New

**Fig. 1** Two different sets of field-aged polymeric insulator samples

2.1 Fourier transform infrared spectroscopy (FTIR)

Fourier transform infrared spectroscopy is a crucial tool for analyzing the material's molecular bonding up to 10- μm surficial depth. The existence of chemical bonds in the compound is represented by the peaks of the FTIR spectrum's transmittance. The changes in the functional group within a given material due to either bond formation or bond breakages can be determined by FTIR. The transmission or absorption characteristics of a given sample can be specified by the vibrational spectrum of a functional group in response to the infrared portion of electromagnetic spectral scanning. Bruker's Tensor II spectrometer with attenuated total reflection (ATR) was used for the FTIR, which involved scanning the materials' surfaces throughout a mid-IR frequency range of 600–4000 cm^{-1} .

2.2 Scanning electron microscopy (SEM) and energy-dispersive X-ray (EDX)

In this study, scanning electron microscopy (SEM) was used to investigate microstructural changes and relative changes

in the surface roughness of the insulator samples. A high-resolution scanning electron microscopy FEI make ESEM QUANTA 200 with energy-dispersive X-ray (EDX) facility at 10–25-kV operating voltage is used. A gold coating (Au) of 20-nm thickness is applied on insulator samples using the sputtering technique (to improve visualization and avoid surface charging). The images from SEM and EDX graphs will clearly show any surface defects or irregularities, as well as offer the individual elemental composition of the sample surface.

2.3 Equivalent salt deposit density (ESDD) and non-soluble deposit density (NSDD)

The site pollution severity of the insulators is determined by measuring equivalent salt deposit density (ESDD) and insoluble materials deposit density (ESDD). ESSD and NSDD measurements were conducted according to IEC TC 36-60815 standard.

2.4 Wettability class measurements

Wettability class measurements are conducted to identify the loss of the water-repelling property due to different electrical and environmental stresses and the aging of the insulator. The spray method is used to assess hydrophobicity in accordance with IEC/TR 62073 [23]. A specific amount of distilled water is sprayed over the housing sheds using a special spray gun. Then, photos are taken and compared with reference images to determine the wettability class.

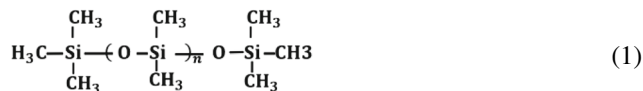
2.5 Tensile strength measurements

The tensile strength measurements were carried out to investigate the mechanical integrity of the field-aged samples. The measurements were conducted using INSTRON 5960 dual column table-top tensile testing system, having a loading capacity of 30 kN. The tensile strength measurement is conducted with cross-head speed at 200 mm/min, which is continued till the samples break/rupture. The test specimen is prepared as per IS 3400, a dumbbell-shaped specimen with a gauge length of 12 mm.

3 Comparative study of field-aged polymer insulators with fresh samples

3.1 FTIR

Functional group changes result from various environmental (dust, rain, light, and heat) and electrical stresses (E-field enhancements, corona, and dry band discharges), leading to aging during the service. In addition, high electrical discharge activities raise the potential of forming new bonds with the ambient molecules, reducing the insulator's life. For FTIR analysis, small cut pieces of V-shaped samples were gathered from the silicone rubber sheds of the high-voltage side of various insulators. Figures 2 and 3 show the FTIR plot of samples obtained from the high-voltage sheds of 400-kV and 132-kV insulators, respectively. Equation 1 shows the chemical structure of silicone rubber (PDMS).



A considerable variation in the transmittance peaks between the aged and new samples is shown in Figs. 2 and 3, indicating the degradation of the samples. A significant decrement in transmittance peak at 1008 cm^{-1} corresponds to the main chain Si–O–Si and at 1260 cm^{-1} corresponds to the side chain Si–CH₃ in the aged samples. A significant change is observed from FTIR plots because of the various discharges that take place at the triple junctions (housing material, air, and metal end-fittings), especially under wet and polluted conditions (droplet-induced discharge and dry band's arcs), and because of the strong ionization of the medium and the ions bombardment on the silicone rubber surface. That is, because the depolymerization of silicone rubber as the energy associated with electrical discharges (corona or dry band discharges) may exceed the polymer matrix bond energy (445 kJ/Mole), resulting in chain scission [24]. Moreover, a large variation is observed in Si–CH₃ peaks in the range between 1270 and 1255 cm^{-1} . This is because the high density of the dry band's arcs near the high-voltage terminal leads to oxidizing of the –Si–CH₃ to the silanol compounds –Si–OH. However, this leads to more rough surface because of the silica forming as a result of the cross-linking of the silanol compounds (–Si–OH) [9], as will be seen in SEM analysis. It has been found that the degree of aging is higher with lower peakiness of the Si–O–Si and Si–CH₃ functional groups. The peaky nature of the Si–O–Si and Si–CH₃ functional groups of samples A1, A2, and A4 is less comparing with the new ones. The transmittance peak at 2961 cm^{-1} corresponds to C–H in CH₃ is less for the aged samples indicating lower methyl content due to the chemical bond breakage. Also, the transmittance peak

at 788 cm^{-1} corresponds to (Si – CH₃)₂ is less for the aged samples, resulting in a lower hydrophobic nature. Both new insulators A3 (400 kV) and A5 (132 kV) show transmittance peaks in the OH region. That is, because aluminum trihydrate (Al (OH)₃) is usually used as a filler in high-temperature vulcanized (HTV) silicone rubber to improve erosion and tracking resistance. It has an OH group inherently in its structure [4]. Various ATH filler loadings result in different transmittance peaks in the OH region $3200\text{--}3700\text{ cm}^{-1}$. As a result, the ATH filler concentration in A3 is higher than in the A5 sample, as the corresponding transmittance peaks are higher in the OH region. A significant decrement in the ATH filler content is observed in the aged samples. This decrement is because of the decomposition of the ATH filler into alumina (Al₂O₃) and water (H₂O) under the effect of electrical discharges.

3.2 SEM and EDX

Any microstructural changes in the surfaces of the insulator samples can be determined using scanning electron microscopy (SEM) images. To investigate the morphological changes over the surface due to aging, samples from the most degraded parts are collected for scanning electron microscopy (SEM) analysis. Figures 4 and 5 show SEM images, EDX graphs, and elemental compositions on the surface of 400-kV and 132-kV insulators, respectively.

The SEM images show that the surface roughness is higher for degraded samples A1, A2, and A4 than for fresh samples A3 and A5. Severe cracks are seen on the surface of aged samples. This rough texture is due to the formation of silica due to the various electrical discharges due to the cross-linking of the silanol compounds [9]. This leads to an increase in the silicon content on the sample's surface from 41.34% in A3 to 48.56% in A1. One more factor that may lead to an increase in the surface roughness is the degradation of the top layer of silicone rubber covering ATH filler particles, thus exposure of ATH particles on the surface [7]. Reactive species such as electrons and free radicals are formed due to high-energy electrical discharges with UV radiation. Certain reactive species, such as the OH radicals with a high oxidation potential, have a destructive impact on the polymer matrix and may result in complete materials breakdown [4]. High-energy discharges lead to oxidation of the SiR, which leads to a significant increment of oxygen content and a decrement in carbon content, where carbon content decreased by more than 61% in A1, 65% in A2, and 16% in A4. At the same time, the oxygen content increased by more than 65% in A1, 41% in A2, and 56% in A4. The ATH filler content is higher in the new 400-kV insulator A3 than in the new 132-kV A5 insulator. Moreover, a significant decrement in the ATH filler content observed in aged samples agrees with the FTIR results. The aluminum content

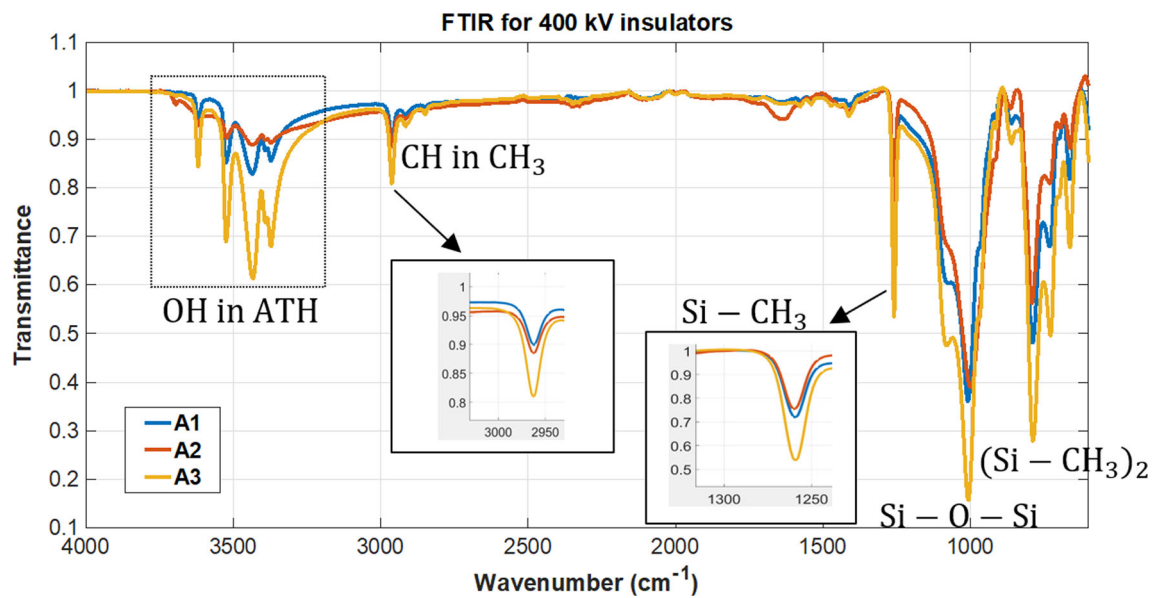


Fig. 2 FTIR plot of samples obtained from the high-voltage sheds of 400-kV insulators

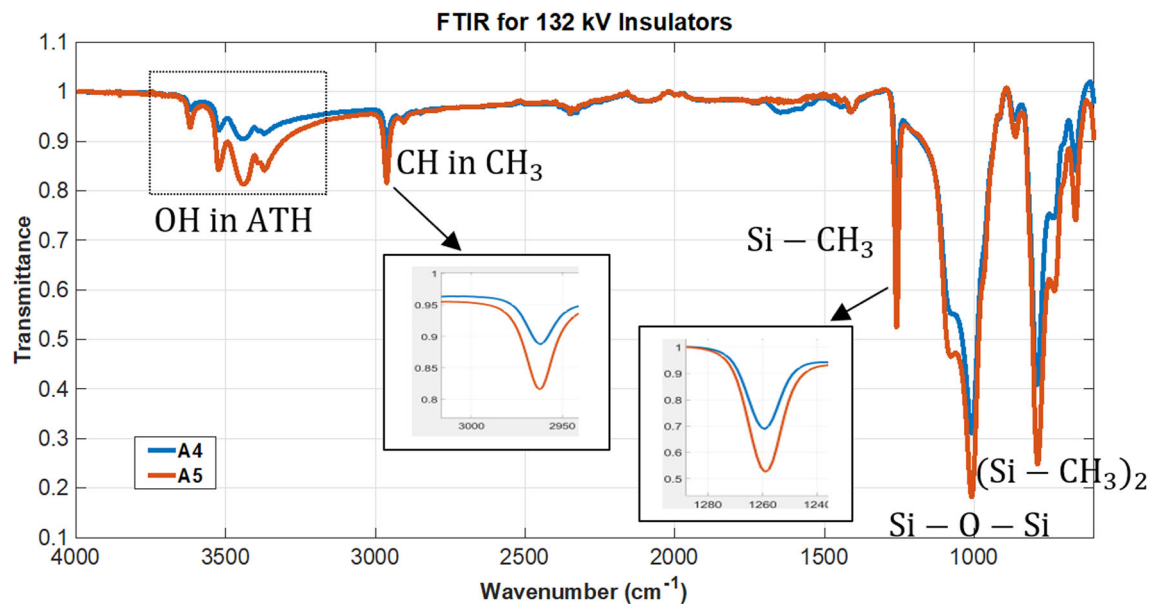
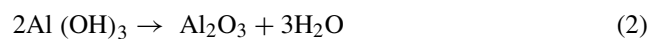


Fig. 3 FTIR plot of samples obtained from the high-voltage sheds of 132-kV insulators

decreased from 23.77% in A3 to 5.63% in A1 and 15.6% in A2. In contrast, it decreased from 18.35% in A5 to 13.59% in A1. ATH filler is decomposed into alumina (Al₂O₃) and water (H₂O) when exposed to high temperatures, as shown in Eq. 2. The produced water lessens the decomposition rate of the polymer by slowing down the temperature rise and dilutes the combustible gas evolved on the polymer [25]. Some minor elements are observed in the aged samples (A1, A2, and A4), such as Mg, Ca, K, and Fe. These could be the salts deposited on the surface due to contamination in

service/pollution interaction.



3.3 ESDD and NSDD

The polymeric insulators' surface indicated the deterioration likely by the pollution in service, which further contributed to the pollution flashover. Non-soluble material deposit (NSDD) and soluble salt deposit (SSD) are the two essential types of contamination. The conductivity of the insulator

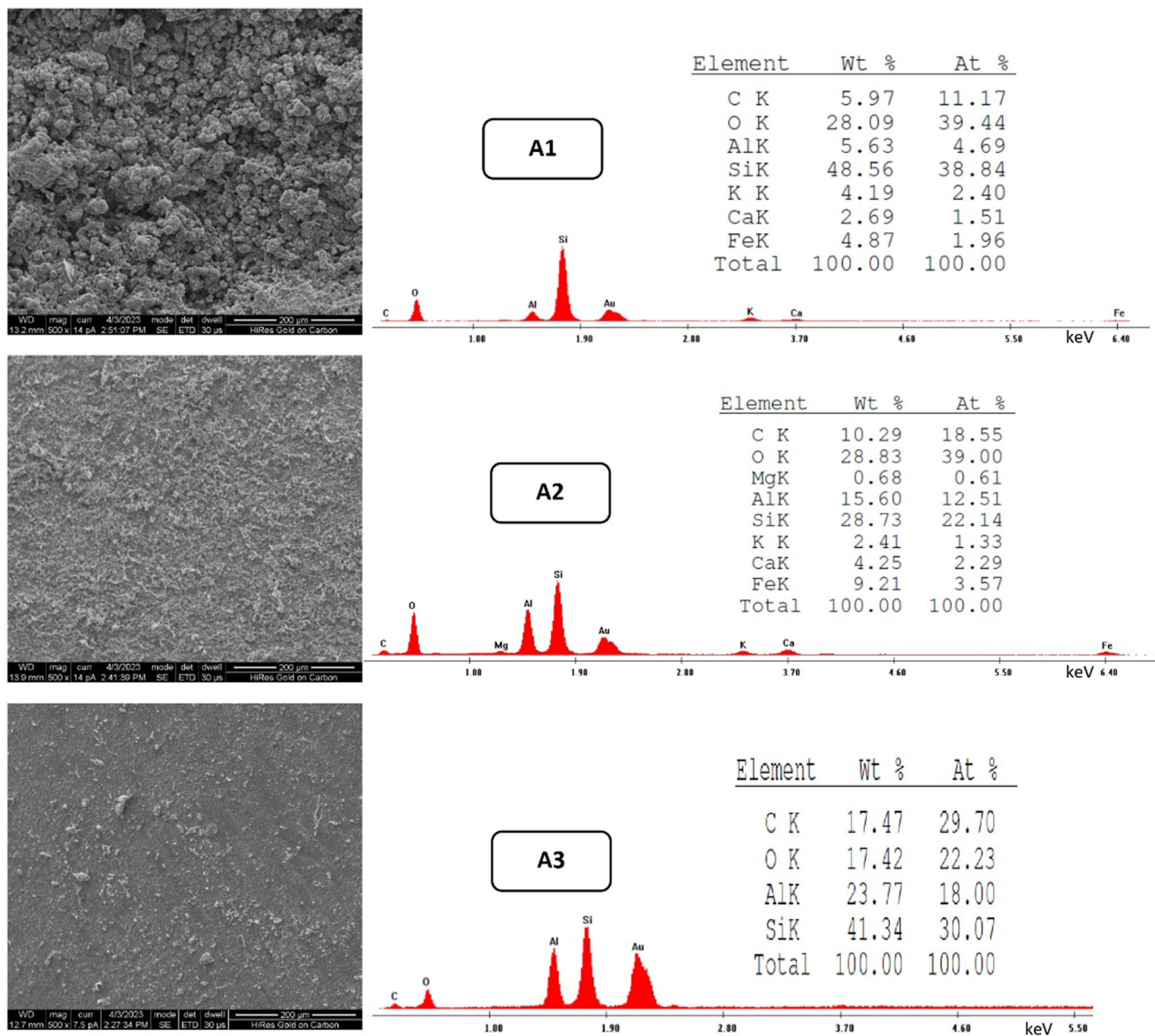


Fig. 4 SEM images of SiR housing samples of 400-kV insulators with EDS graphs and elemental composition

surface increases when deposits, both soluble and insoluble, are present on the polymeric insulator surface. As a result, it raises the leakage current, which accelerates the aging of the insulator and eventually causes a complete flashover. The level of contamination was founded following the evaluation of ESDD measurements. According to the IEC 60587 standard, Table 2 illustrates the relationship between the contamination level and ESDD [26]. The insulators were gently cleaned with distilled water to determine the ESDD, and the resulting solution's conductivity was then measured. A filter paper with a pore size of 2.5 μm was used for filtering the gathered water. Insoluble deposits remaining determine the NSDD, as depicted in Fig. 6. According to IEC TC 36-60815 standard, the investigations were carried out [27]. The

Table 2 The relationship between the contamination level and ESDD [26]

S. No.	ESDD range (mg/cm^2)	Contamination severity
1	0–0.03	Clean or very light
2	0.03–0.06	Light
3	0.06–0.1	Moderate
4	> 0.1	Heavy

distilled water conductivity was 11 $\mu\text{S}/\text{cm}$. Table 3 shows the NSDD and ESDD of samples A2 and A4. The 132-kV field-aged insulator sample A4 had an ESDD level of less than 0.03 mg/cm^2 , which reveals that the insulators

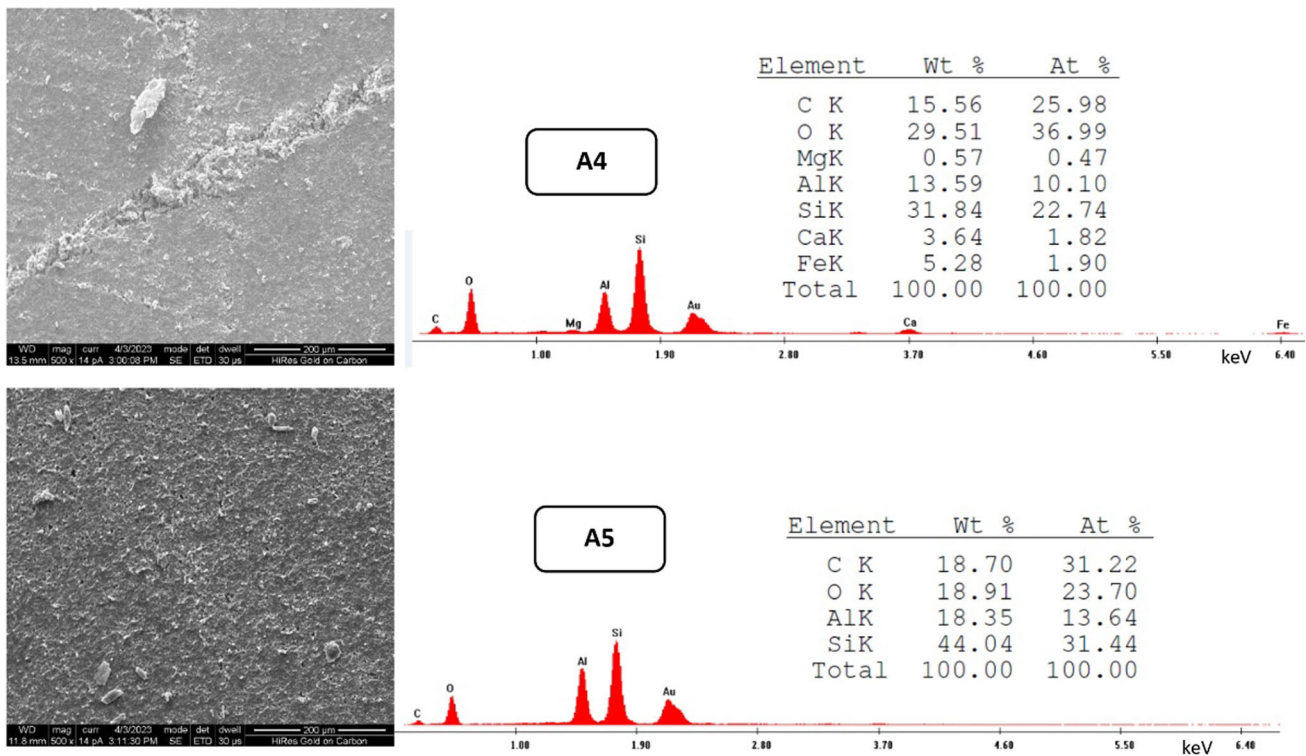


Fig. 5 SEM images of SiR housing samples of 132-kV insulators with EDS graphs and elemental composition



Fig. 6 Non-soluble deposits collected through filter paper for NSDD measurement

Table 3 NSDD and ESDD of the samples A2 and A4

Insulator sample no.	ESDD (mg/cm ²)	NSDD (mg/cm ²)
A2	0.0474	0.7486
A4	0.00437	0.1815

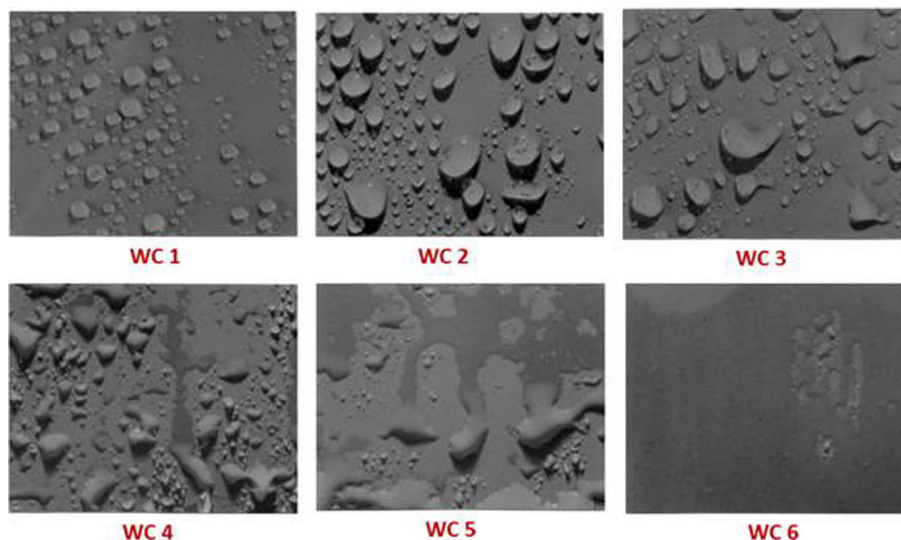
were employed in a light-polluted environment. However, the ESDD level of 400-kV field-aged insulator A2 is in the range of 0.03–0.06 mg/cm². Thus, it was operating in more contaminated conditions. However, there is a potential that

some deposits may be lost while packing and transporting insulators from the field.

3.4 Wettability class measurements

The ability of an insulator to repel water is known as hydrophobicity. The polymer/composite insulators have better hydrophobic properties than conventional ceramic and glass insulators. The wettability class test can be used to identify the loss of the water-repelling property due to different electrical and environmental stresses and the aging of the insulator. The spray method, the contact angle measurement method, and the surface tension method are the three techniques that can be used to assess hydrophobicity in accordance with IEC/TR 62073 [23]. The spray approach was employed in the current experiment to determine the surface hydrophobicity of various samples. Regardless of the test specimen’s size, this approach maintains the test specimen at an angle of 10°–35° with respect to the ground. In this case, a 27° angle has been used. Distilled water with a conductivity of about 14–16 μS/cm was utilized in a particular spray gun with a capacity of 30 ml. The spray gun was used to spray a precise amount of water on the insulator sheds for a specific time. Photos were then taken, and the wettability class according to IEC/TR 62073 was determined by comparing the captured photos to the standard images [23]. Figure 7 shows the various wettability classes as per

Fig. 7 Reference pictures for wettability classes as per standards IEC/TS 62073 [23]



standards. WC1 represents the most hydrophobic surface, and WC6 represents the most hydrophilic surface. Photos of the spray patterns on the housing sheds were captured for each insulator from three angles. The same procedure was repeated for other samples.

Table 4 shows spray patterns captured to determine the wettability class. It was found that the 400-kV old-damaged insulator (A1) belonged to WC4 at the ground, as less than 10% of the observed area is covered with wetted traces from the water runnels and discrete droplets. Whereas at the center and high-voltage side, it belongs to WC5 as more than 10%, and less than 90% of the observed area is covered with wetted traces from the water runnels and discrete droplets. They indicate a significant loss of hydrophobicity of polymer housing material, especially near the HV side, because of the higher electric stress levels. The 400-kV old (A2) insulator belongs to WC3, as the surface of the observed area is covered only by discrete droplets with irregular shapes. However, the new 400-kV insulator (A3) showed a superior hydrophobic nature WC1 as only discrete circular droplets are seen. Both old (A4) and new (A5) 132-kV insulators belong to WC3, as only discrete droplets with irregular shapes are seen.

3.5 Tensile strength measurements

Tensile strength measurements are carried out to analyze the mechanical integrity of the field-aged samples and understand the effect of the various stresses on the mechanical strength. The measurement is conducted using INSTRON 5960 dual column table-top tensile testing system, having a loading capacity of 30 kN. The tensile strength measurement is carried out with cross-head speed at 200 mm/min, which is continued till the samples break/rupture. The test specimen is prepared as per IS 3400, a dumbbell-shaped specimen with a gauge length of 12 mm. The recommended TS values should

range between 2.4 and 60 MPa [28]. Table 5 shows the tensile strength measurements of polymer sheds of field-aged and fresh insulator samples. The average tensile strength values for all the polymer samples except for A1 (400-kV old-damaged) were within the range of acceptance. The ductile nature of housing material (silicone rubber) decreases with increased aging and degradation level. The damaged field-aged sample A1 shows an elongation break percentage reduction of more than 38%.

4 Insulator profile and computation models

The primary purpose of the insulators is to provide electrical isolation between the HV end and the ground and mechanical support to transmission lines. Polymeric outdoor insulators are made up of three essential parts: metallic terminals, insulation housing (silicone rubber), and fiber-reinforced plastic rod. Figure 8 displays the 2D axisymmetric model of the 132-kV composite insulator employed in the present investigation. Table 6 shows all insulator dimensions used in the present study. FRP rod and silicone rubber have relative permittivity of 7.1 and 4.3, respectively. Housing material (SiR) and FRP rod have been assumed to be ideal insulating materials having a too-small conductivity of $1e-15$ S/m. Forged steel terminals with a conductivity of $5.9e7$ S/m are used.

In the 2D axisymmetric model, as the polymeric outdoor insulator is cylindrical, only half of the insulator will be modeled. The practical attachments, such as towers and conductors, are not considered. This model needs less memory and takes less time for computations. The insulator was surrounded by a large enough air space that the field distribution around the insulator was unaffected. The applied voltage (maximum system voltage) on the lower HV electrode is $145/\sqrt{3}$ kV, 50 Hz (RMS), and the upper electrode is

Table 4 Spray pattern captured to determine wettability class





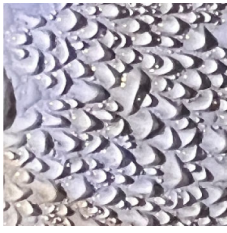

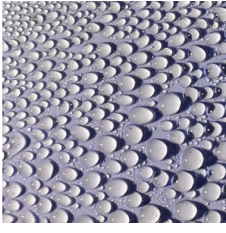


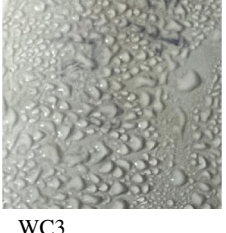


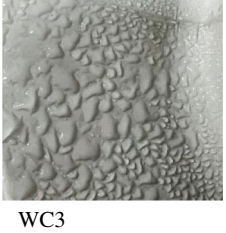
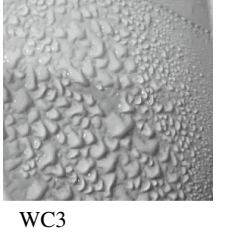

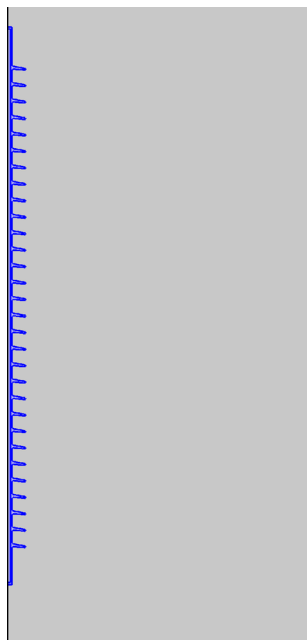
Sample no.	Top shed (GND)	Center shed	Bottom shed (HV)
A1	 WC4	 WC5	 WC5
A2	 WC3	 WC3	 WC3
A3	 WC1	 WC1	 WC1
A4	 WC3	 WC3	 WC3
A5	 WC3	 WC3	 WC3

Table 5 Tensile strength measurements of polymer sheds of field-aged insulator samples

Sample no.	A1	A2	A3	A4	A5
Average tensile strength (MPa)	2.3921	2.8246	3.9030	3.8977	3.9336
Elongation break percentage reduction	38.71%	27.63%	–	0.91%	–

Table 6 Insulator dimensions

Insulator dimensions	Dry arc distance (mm)	Dia of FRP rod (mm)	No. of weather sheds	Dia. of weather sheds (mm)	Thickness of housing (mm)	Creepage distance (mm)
	1238	15	30	90	3	3100

**Fig. 8** Two-dimensional axisymmetric model of 132-kV composite insulator used in the present study

grounded. Along the insulator surface, the mesh density was improved to enhance the simulation accuracy.

A nonlinear frequency solver with the electric currents (ec) interface was used, where inductive effects are negligible. It assumes electromagnetic fields and currents varying slowly. The dynamic electric currents interface is valid if induced electric fields can be ignored [29]. Electric potential V and electric field distribution E are obtained by solving the following equation:

$$-\nabla \cdot (j\omega\epsilon_0\epsilon_r\nabla V) - \nabla \cdot (\sigma\nabla V) = 0 \quad (3)$$

where σ is the electrical conductivity, ϵ_0 is the vacuum permittivity, and ϵ_r is the relative permittivity.

5 Characteristics of nonlinear field grading materials based on ZnO microvaristors

The resistive field grading approach uses a material with special voltage–current characteristics. Consequently, the dominant current is the conduction current. On the other

hand, the displacement current is dominant in capacitive grading approaches such as condenser grading or refractive effect (higher dielectric constant). The resistive grading approach offers more competitive and compact products with increased system voltage levels and more power density. On the other hand, capacitive grading mechanisms under normal working conditions normally lead to an oversized design.

Zinc oxide surge arresters have shown superior performance compared with the preceding overvoltage protection means, which is mainly because of the highly nonlinear voltage–current characteristics and the capability of energy absorption [18]. The recent developments in the compounding of ZnO microvaristors with silicone rubber offer a promising approach for mitigating localized field enhancements in polymeric insulation systems. The concentration of the filler must be larger than the percolation threshold to activate the gradient effect of FGMs and establish a continuous conduction path within FGMs. The switching properties of FGMs could be tailored for any HV application as demanded. Employing various filler concentrations, filler shapes, filler sizes, types of filler, and various housing matrices, the nonlinear switching properties of FGMs could be tuned over a wide range [18–22]. Yang et al. [20] studied the effect of different concentrations of microspherical ZnO varistors (39 and 46.5 vol.%), and the effect of different filler particles diameters filled in silicone rubber on the switching characteristics. The field switching threshold can be modified from 329.4 to 826.5 V/mm. Also, Yang et al. [14] studied the effect of different filler particles' shapes (spherical and irregular) on the switching characteristics. The field switching threshold can be modified over a wider range from 325 to 1731 V/mm and the nonlinearity coefficient from 10 to 15. Tailoring of FGMs switching parameters was recently reviewed in [22].

Compared with conventional field grading materials, the resistive nonlinear FGMs based on ZnO microvaristors offer many advantages. The refractive effect contributes to total electric field grading as it exhibits a larger dielectric constant (10–15). It also exhibits less initial conductivity, thus lower power loss. In addition, it shows faster and sharper nonlinear transitions leading to more efficient stress control under transient conditions [18].

Nonlinear resistive FGMs highly show field-dependent conductivity. At low electric fields, it has extremely low conductivity. The conductivity rapidly rises to a large value when the switching threshold E_b is crossed. The suppression of

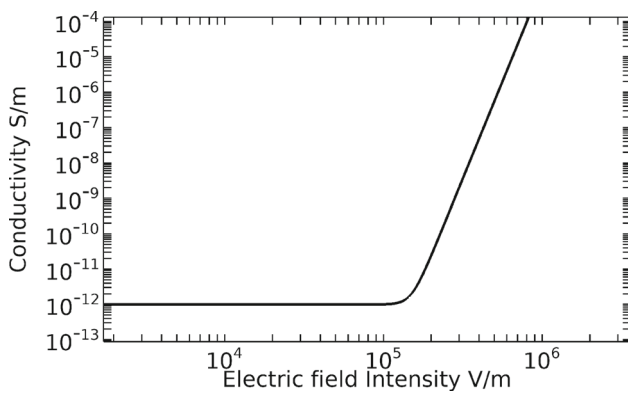


Fig. 9 The nonlinear conductivity of the resistive FGMs employed in the investigation

field enhancements is attained by altering high field regions to the conduction state by raising the FGMs conductivity rapidly. Hence, space charge formation leads to creating a counter field. Consequently, the electric field in high field regions alters itself to a value about E_b . Figure 9 depicts the nonlinear conductivity of the resistive FGMs employed in the investigation. The relationship between the electric field intensity E and the nonlinear conductivity of FGMs is usually defined by the below exponential function:

$$\sigma(E) = \sigma_0 \left[1 + \left(\frac{E}{E_b} \right)^\alpha \right] \quad (4)$$

where σ_0 is the conductivity in low field regions (initial conductivity), α is the nonlinearity coefficient, and E_b is the switching threshold. The dielectric constant of FGMs is assigned as $\epsilon_r = 12$ [30], and the conductivity is assigned as a function of the E-field, $\sigma = f(E)$.

The nonlinear FGMs switching characteristics are essential for efficient E-field grading. The heat generated may result in detrimental thermal consequences in the long-term operation. As long as the active areas of FGMs are confined to a small area, the local resistive grading mechanism could be employed for the long run under normal continuous operation. The main switching parameter is the field switching threshold. An appropriate value of the switching threshold within the limits of the electrical field along the insulator must be chosen to enable its gradient effect. In contrast, selecting a very low value leads to a stress transfer to the end of the FGMs and an increase in the Joule heating. Moreover, the nonlinearity coefficient must be adequately high between 10 and 20 [12].

Because of the limited active regions near both end-fittings, resistive FGMs may operate under continuous normal conditions since low Joule heat is generated as well as a small power loss. The distribution of electric fields along polymeric insulators is normally non-uniform. Figure 10

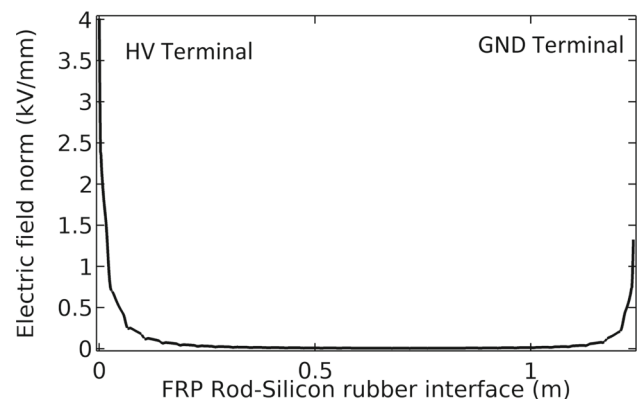


Fig. 10 The electric field distribution along the interface between the FRP rod and the housing material (SiR)

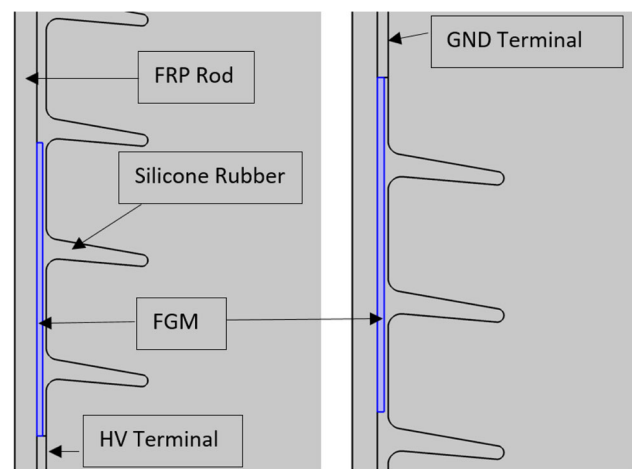


Fig. 11 Composite insulator model with nonlinear FGMs employed in the investigation

exhibits the electric field distribution along the interface between the FRP rod and the housing material (SiR). Field enhancements take place around both terminals, especially near the HV end. However, this enhancement is extended to about 100 mm, and then, E-field becomes more homogeneous. On the FRP rod, two layers of FGMs with a thickness of 2 mm and a length of 100 mm are employed near both end-fittings. They are enclosed within silicone housing to provide protection against different environmental effects, as shown in Fig. 11.

6 Discussion of simulation results

Figure 12 exhibits the electric field along the FRP core-silicone rubber housing with FGM of different field switching thresholds. Low switching thresholds transfer stress to the end of the field grading layer, the field grading layer acts as an

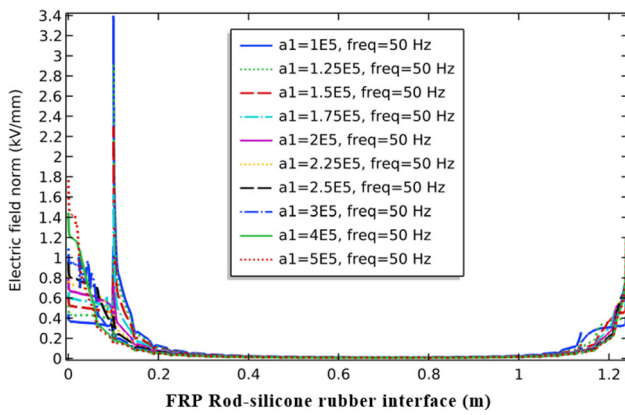


Fig. 12 Electric field along the FRP core-silicone rubber housing with FGM of different field switching thresholds

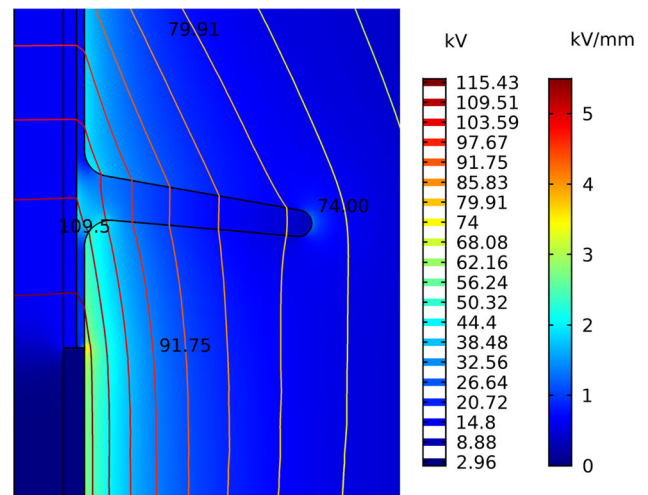


Fig. 14 Equipotential lines distribution as well as the electric field enhancement at the triple junction (HV terminal) with FGM

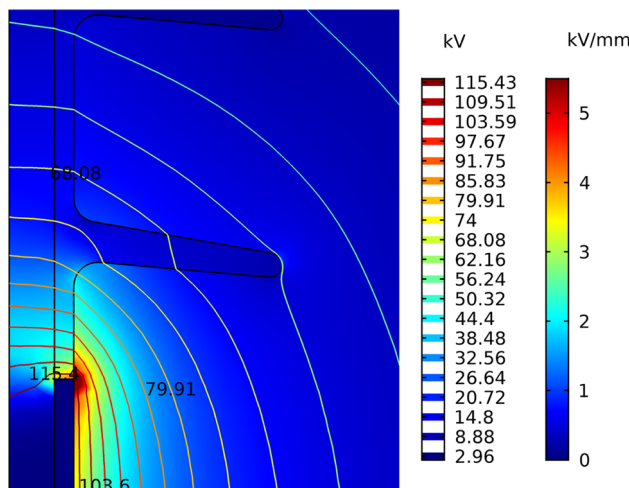


Fig. 13 Equipotential lines distribution as well as the electric field enhancement at the triple junction (HV terminal) without FGM

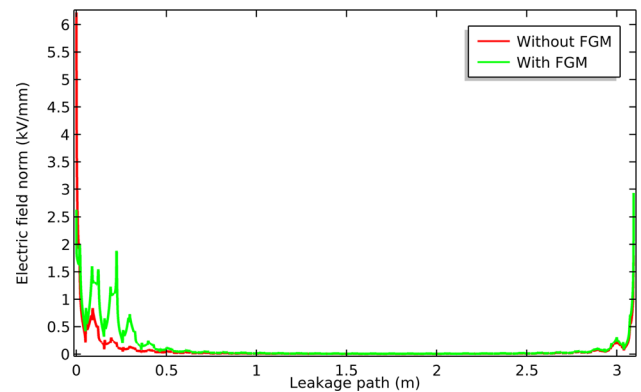


Fig. 15 The electric field distribution along the insulator surface with and without FGM

extension of the terminal and causes localized field enhancements at its end. Whereas with a high switching threshold ($> 4e5$ V/m), the resistive grading effect does not come into action as the electric field that appeared along the FRP rod of the polymeric insulator is less than the switching threshold. The switching threshold of $2e5$ V/m offers the best performance near both ends of the field grading layer. The following switching characteristics will be adopted for all the simulations $\sigma_0 = 1e - 12$ S/m, $E_b = 2e5$ V/m and $\alpha = 10$.

Figure 13 exhibits the distribution of the equipotential lines as well as the electric field enhancement at the triple junction (HV terminal) without FGM. Polymeric insulators exhibit intense E-field enhancements near both end-fittings due to their structure, where the equipotential lines are highly concentrated near both terminals causing these enhancements. Effects of the conductor and other configurations magnify these enhancements near the high-voltage terminal. Adding of FGM layer with appropriate switching

characteristics and design aids to redistribute the concentrated equipotential lines. Once the electric field surpasses the switching threshold of FGMs, the conductivity of the FGMs increases fast and offers a more homogeneous distribution, consequently, significantly decreases the electric field enhancement in critical areas such as triple junctions. Figure 14 shows the distribution of the equipotential lines as well as the electric field enhancement at the triple junction (HV terminal) with FGM.

The electric field along the insulator surface is another crucial factor exhibited in Fig. 15. It shows results that agree with the voltage contours plots. The electric field without FGMs is very strong near end-fittings, especially around the HV electrode. On the other hand, using the FGMs significantly shows improved E-field distribution over the insulator surface, leading to reducing the possibility of surface discharges and the formation of dry bands and their undesirable consequences where the maximum electric field at the triple junction is reduced from 6.22 to 2.63 kV/mm.

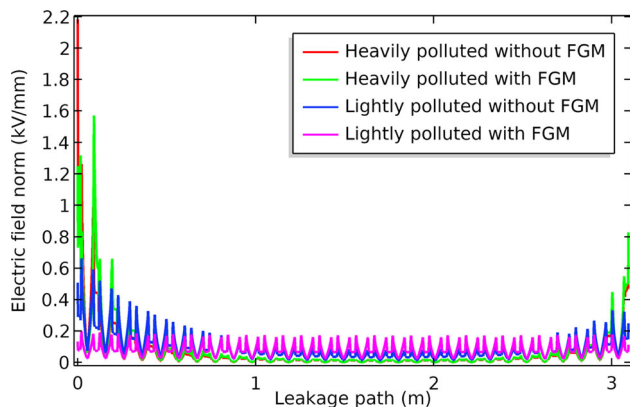


Fig. 16 The electric field distribution along the insulator surface with and without FGM under polluted conditions

Outdoor insulators employed in distribution and transmission power systems are subjected to different environmental conditions. A layer of non-soluble and soluble contaminants is usually formed on the insulator surface. Under wet conditions, this polluted conductive layer increases the leakage current and the power dissipation drastically, consequently, that leads to the formation of dry bands in the high electric field regions and their undesirable consequences. A uniform pollution layer with a thickness of 1 mm is adopted to investigate the insulator performance with FGMs under different polluted severity. Based on the correlation between equivalent salt deposit density and the pollution severity, the pollution layer conductivity is adopted to be less than 175 $\mu\text{S}/\text{cm}$ for light pollution severity and more than 850 $\mu\text{S}/\text{cm}$ for very heavy pollution severity [31]. The pollution layer is assumed to be fully wet with a dielectric constant of 80 and a conductivity of 10 $\mu\text{S}/\text{cm}$ for light pollution severity and 1000 $\mu\text{S}/\text{cm}$ for very heavy pollution severity. The electric field along the insulator surface with and without

FGM under polluted conditions is shown in Fig. 16. It is clear that the E-field enhancements increase as the pollution severity increases. These localized field enhancements and high current density lead to high-power dissipation and water evaporation in these regions, consequently leading to dry band formation and arcs initiations. Using the FGMs significantly shows improved E-field distribution over the insulator surface under different pollution severity, thus reducing the power dissipation and potential of dry band arc initiation and its undesirable consequences. The maximum electric field is decreased from 2.01 to 1.58 kV/mm under very heavy polluted conditions and from 0.65 to 0.2 kV/mm under light-polluted conditions.

The existence of water droplets over the insulator surface leads to excessively E-field enhancements at their extremities due to high relative permittivity (~ 80) compared with air and silicone rubber. These severe E-field enhancements could lead to intense arcs and puncture of the polymeric material, and more severe, it could result in a complete flashover. The electric field distribution with water droplets near the HV terminals is shown in Fig. 17. Adding FGMs significantly reduces these enhancements and offers a more homogeneous field distribution where the maximum electric field is reduced from 20.1 to 11.8 kV/mm.

In addition, a typical lightning impulse 1.2/50 μs of the maximum amplitude (basic insulation level) of 650 kV is applied to the polymeric insulator to evaluate the performance of the FGMs under transient conditions. Figure 18 exhibits the electric field along the insulator surface with and without FGM under the lightning impulse. Field enhancement at the critical areas (triple junction) is excessively high without FGMs, which could result in very severe consequences (complete flashover). Adding FGMs significantly reduces these field enhancements as the conductivity of the

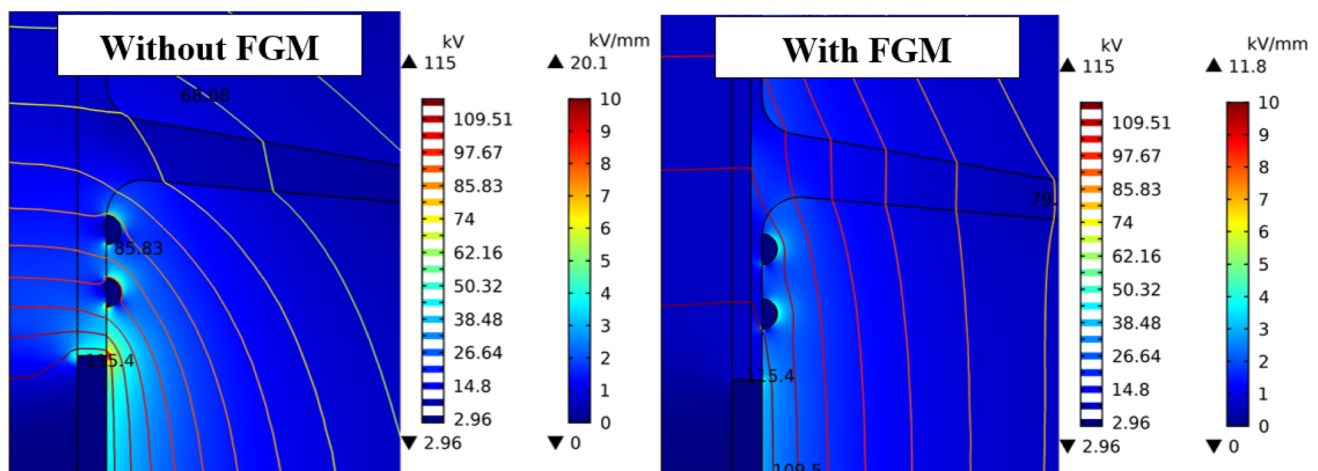


Fig. 17 Equipotential lines distribution as well as the electric field enhancement near the HV terminal with water droplets

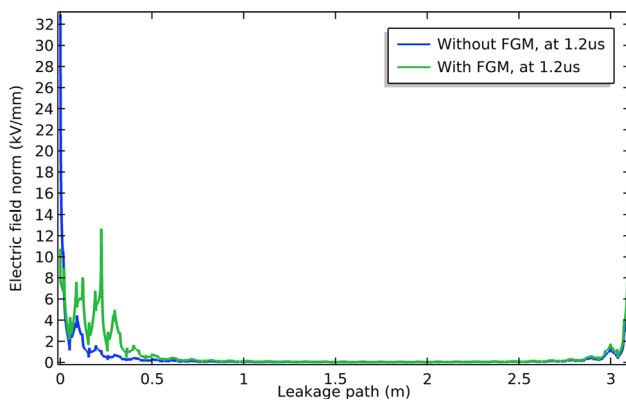


Fig. 18 The distribution of the electric field along the insulator surface with and without FGM under lightning impulse

FGMs increases quickly to a high value. However, the produced Joule heating within the FGMs layer will be very high, which can be neglected for a short time duration. The maximum electric field is reduced from 32.94 to 16.72 kV/mm. These promising results are anticipated to improve the insulator performance under different conditions and reduce the aging and degradation of insulation materials.

7 Summary and conclusions

Experimental investigations on FTIR, SEM, EDX, hydrophobicity measurements, and tensile strength measurements are carried out on the field-aged and fresh polymeric outdoor insulators (132 kV and 400 kV). A significant variation in the transmittance peaks in the FTIR plots is observed for aged insulators, especially the main and side chains. This is due to the depolymerization of SiR housing under the effect of various electrical and environmental stresses. In addition, a significant decrement is in the content of ATH filler in the silicone rubber housing because of the decomposition of the ATH filler into alumina (Al_2O_3) and water (H_2O) under the effect of high-energy electrical discharges. SEM images show severe degradation with rough texture on the aged insulators, especially the damaged 400-kV insulator (A1). EDX graphs show a significant change in the elemental composition on the surface of the samples due to thermal oxidation. The effect of various stresses on the hydrophobic nature of silicone rubber housing was evaluated using the spray technique. A significant loss of hydrophobicity is noticed in the aged samples, especially for the damaged insulator A1. ESDD and NSDD are evaluated to determine the site pollution severity. The tensile strength measurements were conducted to evaluate the mechanical integrity of the aged insulators. The damaged field-aged sample A1 shows an elongation break percentage reduction of more than 38%. Further, a 2D axisymmetric model of the 132-kV insulator

was developed using COMSOL Multiphysics and the finite element method (FEM). One mitigation technique for excessive electric stress was studied using field grading composite (FGM) based on zinc oxide microvaristors. Suitable electrical characteristics and an optimized design of field grading material have been proposed to effectively control the electric stress of the 132-kV polymeric outdoor insulators under different conditions (dry, light, and heavy pollution, with water droplets, and lightning impulse). The results of the simulation demonstrate that using FGMs can significantly improve the performance of polymeric insulators under various operating and environmental, further development of FGM and experimental investigations are planned and in progress.

Author contributions All authors contributed to the study's conception and design. Material preparation, data collection, and analysis were performed by N.R.G. and M.R.H. S.R.B. helped in supervision. Writing—review and editing was performed by M.R.H. All authors reviewed the manuscript.

Funding This declaration is “not applicable.”

Data availability This declaration is “not applicable.”

Declarations

Conflict of interest This declaration is “not applicable.”

Ethical approval This declaration is “not applicable.”

References

- Hackam R (1999) Outdoor HV composite polymeric insulators. *IEEE Trans Dielectr Electr Insul* 6(5):557–585. <https://doi.org/10.1109/TDEI.1999.9286745>
- Verma AR, Reddy BS (2019) Interpretation of surface degradation on polymeric insulators. *Eng Fail Anal* 95:214–225. <https://doi.org/10.1016/j.engfailanal.2018.09.007>
- Meyer LH, Cherney EA, Jayaram SH (2004) The role of inorganic fillers in silicone rubber for outdoor insulation alumina tri-hydrate or silica. *IEEE Electr Insul Mag* 20(4):13–21. <https://doi.org/10.1109/MEI.2004.1318835>
- Papailiou K, Schmuck F (2013) *Silicone composite insulators*. Springer, Berlin, Heidelberg. <https://doi.org/10.1007/978-3-642-15320-4>
- Goudie JL, Owen MJ, Orbeck T (1998) A review of possible degradation mechanisms of silicone elastomers in high voltage insulation applications. In: 1998 Annual report conference on electrical insulation and dielectric phenomena (Cat. No. 98CH36257) (Vol. 1, pp. 120–127). IEEE. <https://doi.org/10.1109/CEIDP.1998.733878>
- Khan Y (2009) Impact of arid desert's simulated environmental conditions on high voltage polymeric insulators. *Am J Eng Appl Sci* 2(2):438–445
- Venkatesulu B, Thomas MJ (2011) Long-term accelerated weathering of outdoor silicone rubber insulators. *IEEE Trans Dielectr Electr Insul* 18(2):418–424. <https://doi.org/10.1109/TDEI.2011.5739445>
- Phillips AJ, Maxwell AJ, Engelbrecht CS, Gutman I (2014) Electric-field limits for the design of grading rings for composite

- line insulators. *IEEE Trans Power Deliv* 30(3):1110–1118. <https://doi.org/10.1109/TPWRD.2014.2362074>
9. Nandi S, Subba BR, Sharma D (2020) Understanding performance of transmission and distribution insulators at very low temperature conditions. *Electr Eng* 102(4):2255–2268. <https://doi.org/10.1007/s00202-020-01019-1>
 10. Tousi MM, Ghassemi M (2020) Combined geometrical techniques and applying nonlinear field dependent conductivity layers to address the high electric field stress issue in high voltage high-density wide bandgap power modules. *IEEE Trans Dielectr Electr Insul* 27(1):305–313. <https://doi.org/10.1109/TDEI.2019.008493>
 11. Roberts A (1995) Stress grading for high voltage motor and generator coils. *IEEE Electr Insul Mag* 11(4):26–31. <https://doi.org/10.1109/57.400761>
 12. Christen T, Donzel L, Greuter F (2010) Nonlinear resistive electric field grading part 1: theory and simulation. *IEEE Electr Insul Mag* 26(6):47–59. <https://doi.org/10.1109/MEI.2010.5599979>
 13. Abd-Rahman R, Haddad A, Harid N, Griffiths H (2012) Stress control on polymeric outdoor insulators using Zinc oxide microvaristor composites. *IEEE Trans Dielectr Electr Insul* 19(2):705–713. <https://doi.org/10.1109/TDEI.2012.6180266>
 14. Yang X, Zhao X, Hu J, He J (2018) Grading electric field in high voltage insulation using composite materials. *IEEE Electr Insul Mag* 34(1):15–25. <https://doi.org/10.1109/MEI.2018.8246118>
 15. Zhao X, Yang X, Hu J, Wang H, Yang H, Li Q, Li X (2019) Grading of electric field distribution of AC polymeric outdoor insulators using field grading material. *IEEE Trans Dielectr Electr Insul* 26(4):1253–1260. <https://doi.org/10.1109/TDEI.2019.007989>
 16. Halloum M R, Sahoo A K, Razouk Y (2021) Control of polymeric outdoor insulators stress by using nonlinear field grading materials. In: 2021 7th international conference on electrical energy systems (ICEES) (pp. 659–664). IEEE. <https://doi.org/10.1109/ICEES51510.2021.9383676>
 17. Halloum M R, Reddy B S, Razouk Y (2021) Optimization of electric field distribution for 33kV polymeric insulator using nonlinear field grading composites. In: 2021 IEEE 5th international conference on condition assessment techniques in electrical systems (CATCON) (pp. 292–297). IEEE. <https://doi.org/10.1109/CATCON52335.2021.9670475>
 18. Donzel L, Greuter F, Christen T (2011) Nonlinear resistive electric field grading part 2: Materials and applications. *IEEE Electr Insul Mag* 27(2):18–29. <https://doi.org/10.1109/MEI.2011.5739419>
 19. Pradhan M, Greijer H, Eriksson G, Unge M (2016) Functional behaviors of electric field grading composite materials. *IEEE Trans Dielectr Electr Insul* 23(2):768–778. <https://doi.org/10.1109/TDEI.2015.005288>
 20. Yang X, He J, Hu J (2015) Tailoring the nonlinear conducting behavior of silicone composites by ZnO microvaristor fillers. *J Appl Polym Sci*. <https://doi.org/10.1002/app.42645>
 21. Gao L, Yang X, Hu J, He J (2016) ZnO microvaristors doped polymer composites with electrical field dependent nonlinear conductive and dielectric characteristics. *Mater Lett* 171:1–4. <https://doi.org/10.1016/j.matlet.2016.02.016>
 22. Can-Ortiz A, Laudebat L, Valdez-Nava Z, Diahm S (2021) Nonlinear electrical conduction in polymer composites for field grading in high-voltage applications: a review. *Polymers* 13(9):1370. <https://doi.org/10.3390/polym13091370>
 23. International Electrotechnical Commission (2016) Guidance on the measurement of wettability of insulator surfaces
 24. Gorur RS, Cherney EA, Burnham JT (1999) Outdoor insulators (pp. 0–9677611). Phoenix: Ravi S. Gorur
 25. Raahauge BE (ed) (2013) Essential readings in light metals: alumina and bauxite. Wiley
 26. International Electrotechnical Commission (2007) Electrical insulating materials used under severe ambient conditions: test methods for evaluating resistance to tracking and erosion
 27. International Electrotechnical Commission (2008) Selection and dimensioning of high-voltage insulators for polluted conditions: part 3: polymer insulators for a.c. systems, Geneva, Switzerland.
 28. Methods of test for vulcanized rubber part 1 determination of tensile stress-strain properties. IS 3400-1
 29. COMSOL Multiphysics (2019) User's Manual. Version 5.5
 30. Halloum MR, Reddy BS, Reddy GN (2022) Stress control for polymeric outdoor insulators using nonlinear resistive field grading materials operating under different conditions. *IEEE Trans Dielectr Electr Insul*. <https://doi.org/10.1109/TDEI.2022.3164857>
 31. Nekahi A, McMeekin S G, Farzaneh M (2015) Effect of pollution severity on electric field distribution along a polymeric insulator. In: IEEE 11th international conference on the properties and applications of dielectric materials (ICPADM) (pp. 612–615). <https://doi.org/10.1109/ICPADM.2015.7295346>.

Publisher's Note Springer Nature remains neutral with regard to jurisdictional claims in published maps and institutional affiliations.

Springer Nature or its licensor (e.g. a society or other partner) holds exclusive rights to this article under a publishing agreement with the author(s) or other rightsholder(s); author self-archiving of the accepted manuscript version of this article is solely governed by the terms of such publishing agreement and applicable law.